

# Direct fabrication of metal-free hollow graphene balls with a self-supporting structure as efficient cathode catalysts of fuel cell

Yanqi Lu · Mingda Liu · Huagui Nie · Cancan Gu ·  
Ming Liu · Zhi Yang · Keqin Yang · Xi'an Chen · Shaoming Huang

Received: 11 January 2016 / Accepted: 19 May 2016 / Published online: 14 June 2016  
© Springer Science+Business Media Dordrecht 2016

**Abstract** Despite the good progress in developing carbon catalysts for oxygen reduction reaction (ORR), the current metal-free carbon catalysts are still far from satisfactory for large-scale applications of fuel cell. Developing hollow graphene balls with a self-supporting structure is considered to be an ideal method to inhibit graphene stacking and improve their catalytic performance. Herein, we fabricated metal-free hollow graphene balls with a self-supporting structure, through using a new strategy that involves direct metal-free catalytic growth from assembly of SiO<sub>2</sub> spheres. To our knowledge, although much researches involving the synthesis of graphene balls have been reported, investigations into the direct metal-free catalytic growth of hollow graphene balls are rare. Furthermore, the electrocatalytic performance shows that the resulting hollow graphene balls

have significantly high catalytic activity. More importantly, such catalysts also possess much improved stability and better methanol tolerance in alkaline media during the ORR compared with commercial Pt/C catalysts. The outstanding performances coupled with an easy and inexpensive preparing method indicated the great potential of the hollow graphene balls with a self-supporting structure in large-scale applications of fuel cell.

**Keywords** Fuel cell · Graphene · Oxygen reduction reaction · Metal-free catalysts · Energy conversion

## Introduction

The large-scale commercial application of fuel cells has been hindered by the high cost, limited supply, and the poor durability of Pt catalysts during the oxygen reduction reaction (ORR) at the cathode (Gong et al. 2009). Much effort has been devoted to the exploration of non-precious metal catalysts with high activity and durability (Yang et al. 2014; Zhong et al. 2014; Cao et al. 2013). These properties should be comparable with those of Pt but at much lower cost. Recently, metal-free nanocarbon materials doped with heteroatoms have drawn attention owing to their striking ORR electrocatalytic performance and relatively low cost (Ye et al. 2014; Chen et al. 2012; Qu et al. 2010; Yao et al. 2012; Yang et al. 2012; Jin et al. 2012). Among

---

**Electronic supplementary material** The online version of this article (doi:10.1007/s11051-016-3457-3) contains supplementary material, which is available to authorized users.

---

Y. Lu · M. Liu · H. Nie (✉) · C. Gu ·  
M. Liu · Z. Yang (✉) · K. Yang · X. Chen ·  
S. Huang (✉)  
Nanomaterials and Chemistry Key Laboratory, Wenzhou  
University, Wenzhou 325027, China  
e-mail: huaguinie@126.com

Z. Yang  
e-mail: yang201079@126.com

S. Huang  
e-mail: smhuang@wzu.edu.cn

these metal-free carbon catalysts, chemically doped graphene is a promising candidate to replace Pt catalysts because of its potentially high surface area, good electronic conductivity, and high electrochemical stability (Qu et al. 2010; Yao et al. 2012; Yang et al. 2012; Jin et al. 2012; Xing et al. 2014; Wang et al. 2011). However, in reality, graphene tends to aggregate and restack. This stacking decreases the effective surface area and restricts catalytic performance, which negatively affects reaction kinetics. Furthermore, poor inter sheet connections between isolated graphene flakes that make up the bulk catalysts break the required continuous pathway for electron transport. This severely limits the intrinsically high conductivity of individual graphene flakes. Recently, much research has been conducted on the inhibition of graphene stacking (Zhao et al. 2014). Developing hollow graphene balls with a self-supporting structure is considered to be an ideal method to solve this issue. Some attempts have been made to fabricate hollow graphene architectures with a self-supporting structure (Yoon et al. 2013; Reina et al. 2009; Wang et al. 2013). This was done using directed chemical vapor deposition (CVD) growth on a metal frame (Chen et al. 2011a, b; Wu et al. 2011) (e.g., Ni foam) or by controlled assembly of graphene (Yoon et al. 2013; Reina et al. 2009; Wang et al. 2013). However, these graphene materials prepared by self-assembly are derived from liquid exfoliated graphene (Hernandez et al. 2008) or reduced graphene oxide (Jeong et al. 2011; Choi et al. 2012; Yu et al. 2008; Reina et al. 2009; Kim et al. 2009). These chemically derived graphene materials usually possess severe structural defects and poor electrical conductivity. Furthermore, the preparation method involving CVD growth on a metal frame also has intrinsic drawbacks such as the use of a relatively expensive metal frame and the requirement for extra steps to remove the metal species. More seriously, the metal particles are usually encapsulated by the so-formed graphene framework and remain in the material even after a tedious removal process. Therefore, the exploitation of a facile and scalable method to simultaneously prepare the ideal hollow graphene balls with high specific surface area and high conductivity in large quantities is still an important challenge.

After comprehensively considering these issues, we developed a new strategy that involves direct metal-free catalytic growth from 3D-assembly of SiO<sub>2</sub>

spheres and achieved the successful fabrication for a hollow graphene balls with a self-supporting structure. Their electrocatalytic performance shows that the resulting hollow graphene balls have significantly high catalytic activity. Additionally, they also possess much improved stability and better methanol tolerance in alkaline media during the ORR compared with commercial Pt/C catalysts. To our knowledge, although much research involving the synthesis of the graphene architectures has been reported, investigations into the direct metal-free catalytic growth of the hollow graphene balls are rare. We believe that the hollow graphene balls with a self-supporting structure and their composites have many potential applications in energy generation or storage, and in photo-electronics fields.

## Experiment section

### Synthesis of the hollow graphene balls with a self-supporting structure

Figure 1 shows a schematic representation of the synthesis procedure used to produce the hollow graphene balls with a self-supporting structure (3D-HGBs). Briefly, SiO<sub>2</sub> nanoparticles (NPs) with different diameters (Fig. S1) were first synthesized by Stober et al.'s (1968) method. They were then self-assembled to form a 3D-assembly of silica colloids using Colvin's method (Jiang et al. 1999). The obtained 3D-assembled silica was heated to

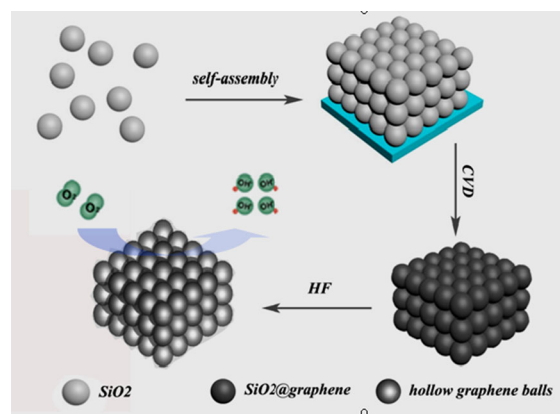


**Fig. 1** Schematic illustration of the synthesis of hollow graphene balls with a self-supporting structure

950–1000 °C in a quartz tube furnace under a high-purity argon atmosphere. Methane gas was then introduced into the quartz tube to deposit carbon on the outer surface of the assembly of SiO<sub>2</sub> NPs. Finally, HF solution was used to dissolve the core SiO<sub>2</sub> NPs to obtain hollow graphene spheres. As a control experiment, hollow graphene balls with different diameters were also produced under the same conditions, and the corresponding transmission electron microscope (TEM) images are shown in Fig. 2. For comparison, graphene balls that were not self-assembled were also treated under the same conditions and the resulting sample was designated HGBs. The physical parameters, electrochemical properties, and corresponding experimental data for these samples are listed in Table 1.

### Electrode preparation

Glassy carbon (GC) electrodes (3 mm diameter, CH instrument Inc.) were polished with a 0.05 and 0.3 μm alumina slurry (CH Instrument Inc.), and subsequently rinsed with ultrapure water and ethanol. To prepare the working electrode, all samples were ultrasonically

dispersed in ethanol under the same process, and equal amounts of each catalyst were dropped onto the GC surface and dried at room temperature, then 0.2 % Nafion was dropped onto the GC and dried at room temperature. For comparison, a commercially available Pt/C-modified GCE (20 % Pt supported on carbon black) was prepared in the same way.

### Electrochemical measurements

The electrochemical measurements of cyclic voltammetry (CV), rotating disk electrode (RDE), and rotating ring-disk electrode (RRDE) were performed by a computer-controlled potentiostat (CHI760C) with a three-electrode cell system. A glass carbon RDE after loading the electrocatalyst was used as the working electrode, an Ag/AgCl (KCl, 3 M) electrode as the reference electrode, and a Pt wire as the counter electrode. The electrochemical experiments were conducted in O<sub>2</sub>-saturated 0.1 M KOH electrolyte for the oxygen reduction reaction. The potential was cyclically scanned between −0.8 and +0.2 V at room temperature after purging O<sub>2</sub> or N<sub>2</sub> gas for 30 min. RDE measurements were conducted at different

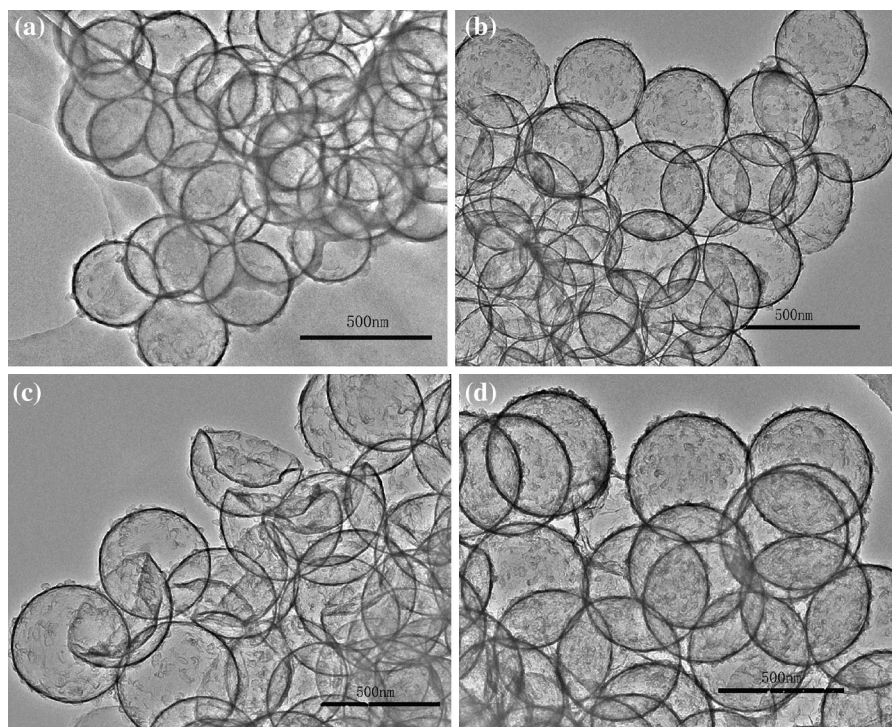


**Fig. 2** Typical TEM images of HGBs with different diameters **a** 360 nm, **b** 400 nm, **c** 450 nm, **d** 550 nm

**Table 1** Physical parameters, electrochemical properties, and corresponding experimental data for the hollow graphene balls of different annealing temperatures

Sample	Annealing temperature (°C)	Peak potential	Peak current	Number of electron transfer
3D-950HGBs	950	−0.376	275.0	2.7
3D-960HGBs	960	−0.354	325.6	3.2
3D-975HGBs	975	−0.386	282.5	2.23
3D-1000HGBs	1000	−0.391	244.2	2.19
960HGBs	960	−0.364	218.1	3.02

rotating speeds from 1225 to 2500 rpm, and RRDE measurements were carried out at 1600 rpm.

The electron transfer number ( $n$ ) was determined from RRDE measurement on the basis of the disk current ( $I_D$ ) and ring current ( $I_R$ ) via the following equation:

$$N = 4I_D / (I_D + I_R/N),$$

where  $N = 0.36$  is the current collection efficiency of Pt ring.

## Results and discussion

Figure 3a shows a typical scanning electron microscopy (SEM) image of the SiO<sub>2</sub> NPs. As shown in Fig. 3a, these spheres of uniform dimension with a mono-disperse size distribution can be seen. Their diameters could be adjusted by varying the concentration of tetraethyl orthosilicate. Corresponding SEM images of these SiO<sub>2</sub> NPs with different diameters are shown in Fig. S1. Figure 3b shows an image of a 3D-assembly of silica colloids after using Colvin's method. In comparison with Fig. 3a, the 3D assembly of the silica colloids exhibits a well-organized arrangement of SiO<sub>2</sub> NPs. The optical image of the sample in Fig. 3c confirms that a white macroscopic film forms after the SiO<sub>2</sub> NPs were self-assembled. After carbon deposition, a black film can be obtained as shown in Fig. 3d. Figure 3e shows a SEM image of the black film with a thickness of about 600 μm. The SEM (Fig. 3f, g) and TEM images (Fig. 3h, i) clearly reveal that the black film is composed of graphene balls with a hollow structure. The high-resolution TEM image in the upper right of Fig. 3h shows a typical lattice fringe spacing of 0.34 nm, corresponding to the spacing between two (002) planes of

graphite, which confirms the formation of multilayer graphene (Sheng et al. 2011). To further probe the graphene structure, wide angle powder X-ray diffraction (Fig. 4a) and Raman spectroscopy (Fig. 4b) measurements were carried out. From Fig. 4a, the pattern of 3D-960HGBs revealed a typical peak at 26° that was attributed to the (002) plane of graphite (Lee et al. 2013). The Raman spectrum in Fig. 4b shows a higher  $I_D/I_G$  ratio and a clear 2D peak was also detected, which implies that direct metal-free catalytic growth from the SiO<sub>2</sub> spheres can favor the efficient synthesis of graphene balls, despite the fact that the synthesized graphene layers had defective structures (Yoon et al. 2012). Figure 4c shows the N<sub>2</sub> adsorption/desorption isotherms of the 3D-960HGBs, which shows a type IV adsorption–desorption behavior. Using the multi-point Brunauer–Emmett–Teller method, the specific surface area of the 3D-960HGBs extracted is 325.9 m<sup>2</sup> g<sup>−1</sup>. The limited adsorption of N<sub>2</sub> at the lower  $P/P_0$  region as well as the quick uptake of N<sub>2</sub> at higher pressure ( $P/P_0 > 0.9$ ) in the N<sub>2</sub> adsorption–desorption isotherm suggests that the most of contributes to the surface area of 3D-960HGBs may be originated from the external part of the graphene balls. Of course, some contributes due to the internal part cannot still be ignored. Furthermore, from Table S1, it can be found that the surface areas and pore volumes for these 3D-HGBs samples obtained at different temperatures gradually decrease as the annealing temperature changes from 950 to 1000 °C. It is speculated that the major reason for this phenomenon may be due to the reduction of pores originating in the formation of more graphite crystals at higher temperature. The X-ray photoelectron spectroscopy (XPS) survey spectrum of the 3D-960HGBs (Fig. 4d) distinctly shows the presence of C 1s and O 1s peaks without any other signals. This further

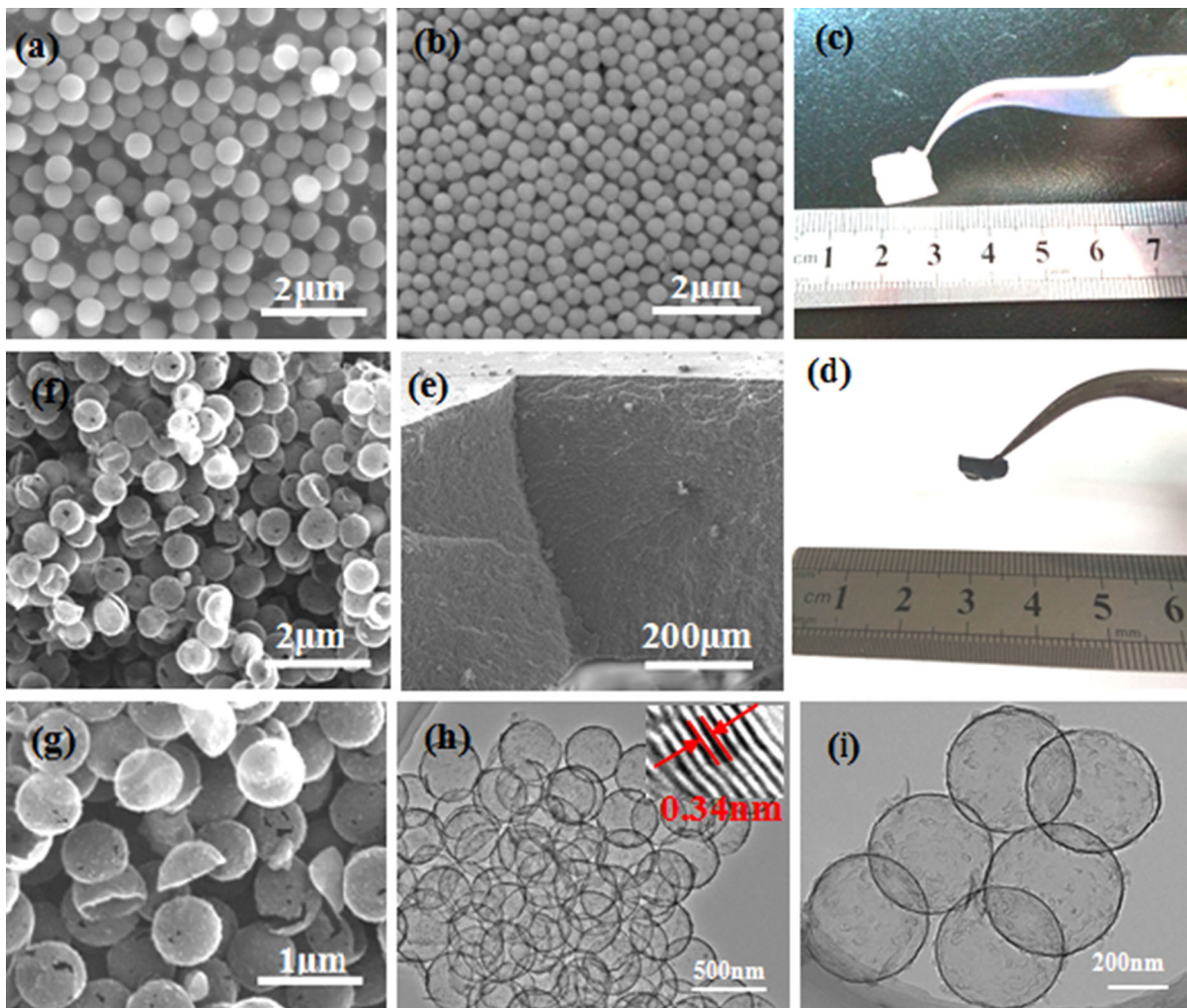


**Fig. 3** **a** SEM image of  $\text{SiO}_2$ , **b** SEM image of 3D assembly  $\text{SiO}_2$ , **c** photograph of 3D  $\text{SiO}_2$ , **d** Photograph of 3D-960HGBs, **e, f** SEM image of 3D-960HGBs, **g** Magnification SEM image of

3D-960HGBs, **h, i** TEM images of 3D-960HGBs, the inset confirms a typical lattice fringe spacing of 0.34 nm

demonstrates that the  $\text{SiO}_2$  template was effectively removed leaving only hollow graphene spheres.

Considering that the annealing temperature is an important factor in determining the growth of graphene, we investigated the effect of annealing temperature on the morphology of these hollow graphene balls (3D-HGBs). The resulting samples were denoted 3D-950HGBs, 3D-960HGBs, 3D-975HGBs, and 3D-1000HGBs. From the obtained photographs of these HGBs and 3D-HGBs shown in Figs. S2 and S3, the color of these HGBs and 3D-HGBs deepened in proportion to the annealing temperature from light gray to brown to black. The high-

resolution TEM images in Fig. S4 clearly show that the number of graphene layers increases with the annealing temperature. Thermogravimetry monitoring of the oxidation that occurred in air indicates that the degree of graphitization of the HGBs increases with annealing temperature (Fig. S5). The content distribution data for various HGBs are listed in Table S2. This result is consistent with the previous result concerning the influence of annealing temperature on the formation of graphene layers. These results indicate that our approach to the growth of 3D-HGBs, with control over the diameter and the thickness of the graphene layer, was successful.

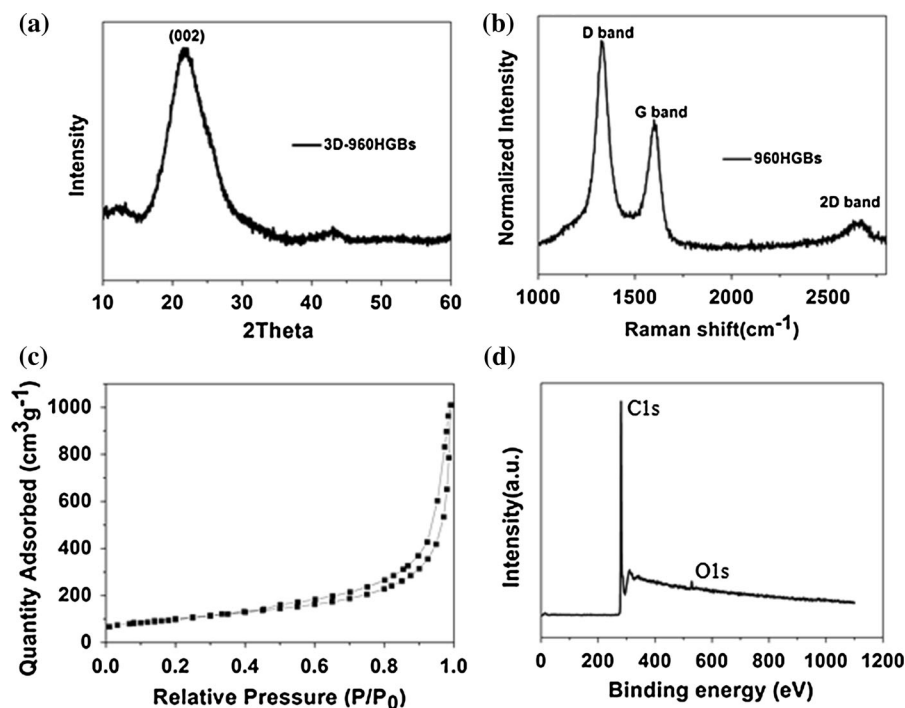


**Fig. 4** **a** X-ray diffraction patterns of 3D-960HGBs, **b** Raman spectrum of 3D-960HGBs at a laser excitation wavelength of 633 nm, **c** nitrogen adsorption/desorption isotherms of 3D-960HGBs, **d** the survey XPS spectra of 3D-960HGBs

As a demonstration of the potential of 3D-HGBs, the performance of the 3D-HGB sample as a true metal-free catalyst for the oxygen reduction reaction was studied using CV in a 0.1 M KOH solution saturated with  $N_2$  or  $O_2$ . Figure 5a clearly shows the ORR peaks for all the samples (3D-950HGBs, 3D-960HGBs, 3D-975HGBs, 3D-1000HGBs) under  $O_2$ -saturated conditions. Compared with the 3D-950HGBs electrode, 3D-975HGBs electrode, 3D-1000HGBs electrode, the 3D-960HGBs showed a slightly positive shift in terms of ORR peak potential and a more pronounced increase in ORR current. To gain further insight into the ORR performance of these samples, we also performed linear sweep voltammetry measurements (LSV) using a RDE at a rotation rate of 2500 rpm. Figure 5b shows that the 3D-960HGBs have a more positive onset potential and a higher limiting current density than the 3D-950HGBs, the 3D-975HGBs, and the 3D-1000HGBs. This result further supports the CV observations. Furthermore, from Fig. 5b, it can be seen that the current density ( $-0.5$  V) of the 3D-960HGBs is close to that of the Pt/C catalyst, though the onset potential is slightly

negative. These results suggest that the ORR catalytic activity of the 960HGBs is comparable with that of the previously reported metal-free carbon catalysts (Ye et al. 2014; Chen et al. 2012; Qu et al. 2010; Yao et al. 2012; Yang et al. 2012). To further determine the advantages of these 3D self-assembling structures in terms of electronic transport and catalytic performance, graphene balls that did not undergo self-assembling treatment (960HGBs) were prepared under the same conditions. Their CV characterization is shown in Fig. 5c, where the peak potential for the 3D-960HGBs electrode shifted positively to  $-0.354$  V and its oxygen reduction current was found to be  $325.6$   $\mu$ A after correcting for the background current. This was obviously higher than that of the 960HGBs electrode ( $218.1$   $\mu$ A). To further confirm the role of 3D-960HGBs in the ORR electrochemical process, we also performed RDE measurements at a rotation rate of 2500 rpm (Fig. 6). Furthermore, an impedance test was also carried out over a frequency range of 100 kHz–0.01 Hz, as shown in Fig. 5d. The 3D-960HGBs gave a smaller semicircle plot, which means that it has a lower resistivity than the 960HGBs.

**Fig. 5** **a** CVs for various 3D-HGBs obtained under different temperatures, **b** LSV curves for various 3D-HGBs and a Pt/C catalyst on a glass carbon rotating disk electrode saturated in O<sub>2</sub> at a rotation rate of 2500 rpm, **c** CV curves for 3D-960HGBs and 960HGBs, **d** electrochemical impedance spectroscopy of 3D-960HGBs and 960HGBs, **e** chronoamperometric responses of 3D-960HGBs with 3 M methanol added at around 100 s, **f** current–time (*i*–*t*) chronoamperometric response of the 3D-960HGBs and Pt/C electrode at –0.35 V in an O<sub>2</sub>-saturated 0.1 M KOH solution

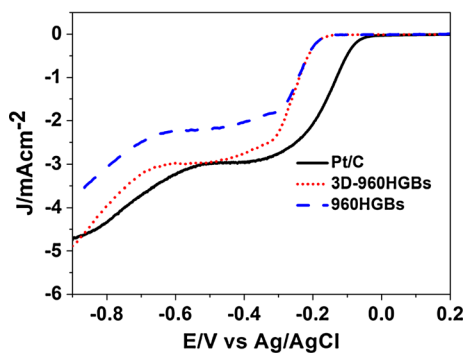
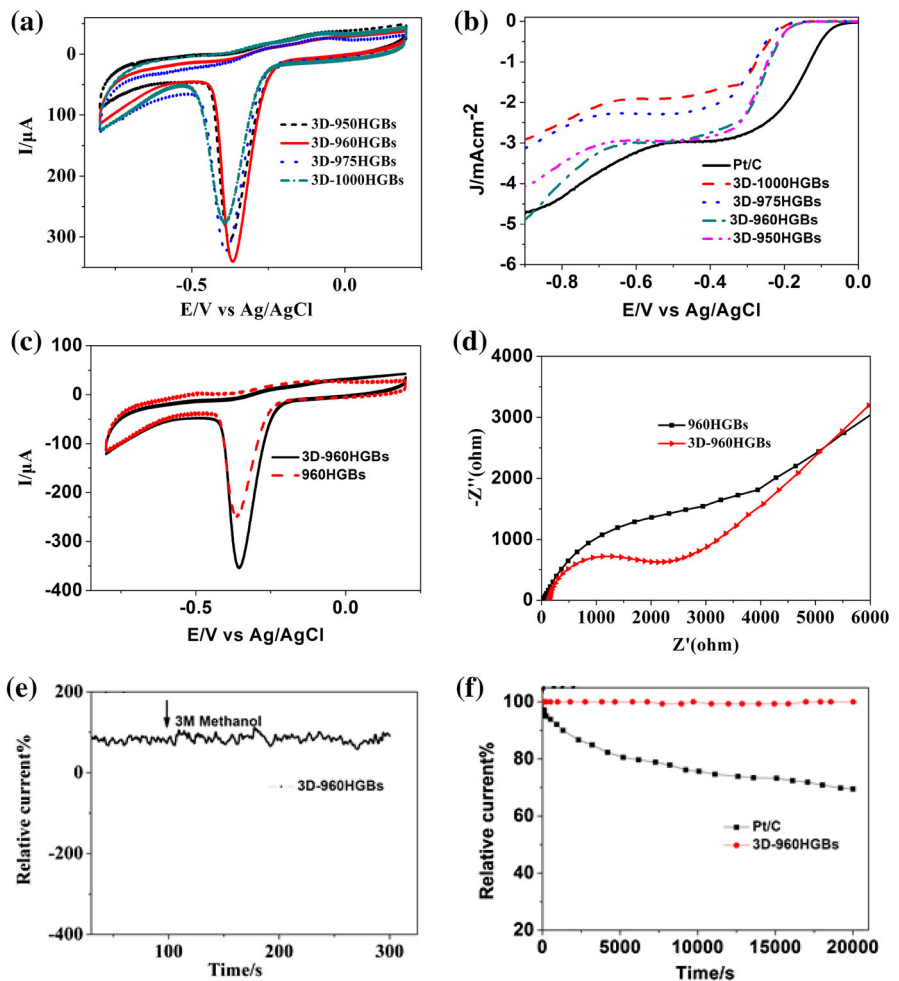


**Fig. 6** LSV curves for 3D-960HGBs, 960HGBs, and Pt/C catalyst at a rotation rate of 2500 rpm

All these results are in agreement with the superior ORR performance of the 3D-960HGBs compared with the 960HGBs. The excellent performance observed

for the 3D-960HGBs sample can be attributed to the effective use of its large specific surface area and high electrical conductivity. Additionally, the 3D self-assembling structure ensures the highly efficient transport of electrons, electrolytic ions, and intermediate reactants. To further confirm the role of the 3D-960HGBs in the ORR electrochemical process, we also carried out RRDE voltammetry (see Fig. 7). The electron transfer number (*n*) for the 3D-960HGBs was calculated to be 3.2 (Fig. S6) and this indicates a primary four electron transfer reaction. The electrocatalytic activity of the 3D-960HGBs was comparable with that of other non-Pt catalysts in alkaline electrolytes (Qu et al. 2010; Yao et al. 2012; Yang et al. 2012; Jin et al. 2012). These results further confirm that 3D-HGB is a promising non-Pt material with high catalytic activity for the ORR.

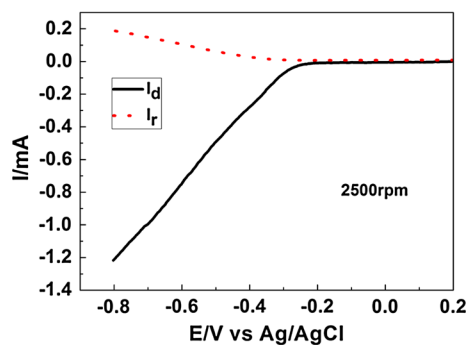


**Fig. 7** RRDE voltammeteries of ORR for 3D-960HGBs in  $O_2$ -saturated  $0.1 \text{ mol L}^{-1}$  KOH electrolyte at a rotation rate of 2500 rpm and a scan rate of  $5 \text{ mV s}^{-1}$

Possible crossover effects and the stability of the catalyst materials are both important parameters for an evaluation of their practical application in fuel cells. Therefore, their chronoamperometric response toward methanol that was introduced into an  $O_2$ -saturated electrolyte was measured for the 3D-960HGBs. Figure 5e shows that after the addition of 3 M methanol at 100 s, no noticeable change is apparent in the ORR current for the 3D-960HGBs electrode, while the ORR current of the Pt/C catalyst showed sharp attenuation (Yang et al. 2012). These results indicate that the 3D-960HGB exhibits high ORR selectivity and has a good ability to avoid crossover effects. The durability of the 3D-960HGBs and the Pt/C catalysts was also compared. Figure 5f shows that the resulted  $i-t$  chronoamperometric response for 3D-960HGB exhibited very slow attenuation, and a high relative current of 99.4 % still persisted after 20,000 s. In contrast, the Pt/C electrode exhibits a gradual decrease with a current loss of approximately 71.5 % after 20,000 s. These results confirm that the 3D-960HGBs is a promising metal-free catalyst for use in methanol and alkaline fuel cells.

## Conclusion

In summary, we developed a new strategy that involves direct metal-free catalytic growth from  $SiO_2$  spheres for the fabrication of hollow graphene balls with a self-supporting structure. These materials feature significant electrocatalytic activity, long-term stability, and an excellent resistance to crossover effects during the ORR. The outstanding performance

of the 3D assembly of the hollow graphene balls fabricated in an easy and inexpensive method suggests a straightforward route toward the achievement of textured graphene. These materials can potentially be used in electronic devices as well as in other energy-related applications.

**Acknowledgments** This work was supported in part by grants from NSFC (21273163, 51572197, 21475096, 51420105002, and 51202165).

## References

- Cao RG, Thapa RJ, Kim HJ, Xu XD, Kim MG, Li Q, Park NJ, Liu ML, Cho J (2013) Promotion of oxygen reduction by a bio-inspired tethered iron phthalocyanine carbon nanotube-based catalyst. *Nat Commun* 4:2076. doi:[10.1038/ncomms3076](https://doi.org/10.1038/ncomms3076)
- Chen SS, Cai WW, Piner RD, Su JW, Wu YP, Ren YJ, Kang JY, Ruoff RS (2011a) Synthesis and characterization of large-area graphene and graphite films on commercial Cu-Ni alloy foils. *Nano Lett* 11:3519–3525. doi:[10.1021/nl201699j](https://doi.org/10.1021/nl201699j)
- Chen ZP, Ren WC, Gao LB, Liu BL, Pei SF, Cheng HM (2011b) Three-dimensional flexible and conductive interconnected graphene networks grown by chemical vapour deposition. *Nat Mater* 10:424–428. doi:[10.1038/nmat3001](https://doi.org/10.1038/nmat3001)
- Chen S, Bi JY, Zhao Y, Yang LJ, Zhang C, Ma YW, Wu Q, Wang XZ, Hu Z (2012) Nitrogen-doped carbon nanocages as efficient metal-free electrocatalysts for oxygen reduction reaction. *Adv Mater* 24:5593–5597. doi:[10.1002/adma.201202424](https://doi.org/10.1002/adma.201202424)
- Choi BG, Yang MH, Hong WH, Choi JW, Huh YS (2012) 3D macroporous graphene frameworks for supercapacitors with high energy and power densities. *ACS Nano* 5:4020–4028. doi:[10.1021/nn3003345](https://doi.org/10.1021/nn3003345)
- Gong KP, Du F, Xia ZH, Durstock M, Dai LM (2009) Nitrogen-doped carbon nanotube arrays with high electrocatalytic activity for oxygen reduction. *Science* 323:760–764. doi:[10.1126/science.1168049](https://doi.org/10.1126/science.1168049)
- Hernandez Y, Nicolosi V, Lotya M, Blighe FM, Sun ZY, De S, McGovern IT, Holland B, Byrne M, Gun'ko YK, Boland JJ, Niraj P, Duesberg G, Krishnamurthy S, Goodhue R, Hutchison J, Scardaci V, Ferrari AC, Coleman HN (2008) High-yield production of graphene by liquid-phase exfoliation of graphite. *Nat Nanotech* 3:563–568. doi:[10.1038/nnano.2008.215](https://doi.org/10.1038/nnano.2008.215)
- Jeong HM, Lee JW, Shin WH, Choi YJ, Shin HJ, Kang JK, Choi JW (2011) Nitrogen-doped graphene for high-performance ultracapacitors and the importance of nitrogen-doped sites at basal planes. *Nano Lett* 6:2472–2477. doi:[10.1021/nl2009058](https://doi.org/10.1021/nl2009058)
- Jiang P, Bertone JF, Hwang KS, Colvin VL (1999) Single-crystal colloidal multilayers of controlled thickness. *Chem Mater* 8:2132–2140. doi:[10.1021/cm990080+](https://doi.org/10.1021/cm990080+)
- Jin ZP, Nie HG, Yang Z, Zhang J, Liu Z, Xu XJ, Huang SM (2012) Metal-free selenium doped carbon

- nanotube/graphene networks as a synergistically improved cathode catalyst for oxygen reduction reaction. *Nanoscale* 4:6455–6460. doi:[10.1039/C2NR31858J](https://doi.org/10.1039/C2NR31858J)
- Kim KS, Zhao Y, Jang H, Lee SY, Kim JM, Kim KS, Ahn JH, Kim P, Choi JY, Hong BH (2009) Large-scale pattern growth of graphene films for stretchable transparent electrodes. *Nature* 7230:706–710. doi:[10.1038/nature07719](https://doi.org/10.1038/nature07719)
- Lee JS, Kim SI, Yoon JC, Jang JH (2013) Chemical vapor deposition of mesoporous graphene nanoballs for supercapacitor. *ACS Nano* 7:6047–6055. doi:[10.1021/nn401850z](https://doi.org/10.1021/nn401850z)
- Qu LT, Liu Y, Beak JB, Dai LM (2010) Nitrogen-doped graphene as efficient metal-free electrocatalyst for oxygen reduction in fuel cells. *ACS Nano* 4:321–1326. doi:[10.1021/nn901850u](https://doi.org/10.1021/nn901850u)
- Reina A, Jia XT, Ho J, Nezich D, Son HB, Bulovic V, Dresselhaus MS, Kong J (2009) Large area, few-layer graphene films on arbitrary substrates by chemical vapor deposition. *Nano Lett* 9:30–35. doi:[10.1021/nl801827v](https://doi.org/10.1021/nl801827v)
- Sheng ZH, Shao L, Chen JJ, Bao WJ, Wang FB, Xia XH (2011) Catalyst-free synthesis of nitrogen-doped graphene via thermal annealing graphite oxide with melamine and its excellent electrocatalysis. *ACS Nano* 6:4350–4358. doi:[10.1021/nn103584t](https://doi.org/10.1021/nn103584t)
- Stober W, Fink A, Bohn E (1968) Controlled growth of monodisperse silica spheres in the micron size range. *J Colloid Interface Sci* 1:62–69. doi:[10.1016/0021-9797\(68\)90272-5](https://doi.org/10.1016/0021-9797(68)90272-5)
- Wang SY, Yu DS, Dai LM, Chang DW, Beak JB (2011) Polyelectrolyte-functionalized graphene as metal-free electrocatalysts for oxygen reduction. *ACS Nano* 5:6202–6209. doi:[10.1021/nn200879h](https://doi.org/10.1021/nn200879h)
- Wang XB, Zhang YJ, Zhi CY, Wang X, Tang DM, Xu YB, Weng QH, Jiang XF, Metome M, Golberg D, Bando Y (2013) Three-dimensional strutted graphene grown by substrate-free sugar blowing for high-power-density supercapacitors. *Nat Commun* 4:2905. doi:[10.1038/ncomms3905](https://doi.org/10.1038/ncomms3905)
- Wu W, Jauregui LA, Su ZH, Liu ZH, Bao JM, Chen YP, Yu QK (2011) Growth of single crystal graphene arrays by locally controlling nucleation on polycrystalline Cu using chemical vapor deposition. *Adv Mater* 23:4898–4903. doi:[10.1002/adma.201102456](https://doi.org/10.1002/adma.201102456)
- Xing T, Zheng Y, Li LH, Cowie BCC, Gunzelmann D, Qiao SZ, Huang SM, Chen Y (2014) Observation of active sites for oxygen reduction reaction on nitrogen-doped multilayer graphene. *ACS Nano* 8:6856–6862. doi:[10.1021/nn501506p](https://doi.org/10.1021/nn501506p)
- Yang Z, Yao Z, Li GF, Fang GY, Nie HG, Liu Z, Zhou XM, Chen XA, Huang SM (2012) Sulfur-doped graphene as an efficient metal-free cathode catalyst for oxygen reduction. *ACS Nano* 6:205–211. doi:[10.1021/nn203393d](https://doi.org/10.1021/nn203393d)
- Yang Z, Zhou XM, Jin ZP, Liu Z, Nie HG, Chen XA, Huang SM (2014) A facile and general approach for the direct fabrication of 3D vertically aligned carbon nanotube array/transition metal oxide composites as non-Pt catalysts for oxygen reduction reactions. *Adv Mater* 26:3156–3161. doi:[10.1002/adma.201305513](https://doi.org/10.1002/adma.201305513)
- Yao Z, Nie HG, Yang Z, Zhou XM, Liu Z, Huang SM (2012) Catalyst-free synthesis of iodine-doped graphene via a facile thermal annealing process and its use for electrocatalytic oxygen reduction in an alkaline medium. *Chem Commun* 48:1027–1029. doi:[10.1039/C2CC16192C](https://doi.org/10.1039/C2CC16192C)
- Ye TN, Lv LB, Li XH, Xu M, Chen JS (2014) Strongly veined carbon nanoleaves as a highly efficient metal-free electrocatalyst. *Angew Chem Int Ed* 53:6905–6909. doi:[10.1002/anie.201403363](https://doi.org/10.1002/anie.201403363)
- Yoon SM, Choi WM, Baik H, Shin HJ, Song I, Kwon MS, Bae JJ, Kim H, Lee YH, Choi JY (2012) Synthesis of multilayer graphene balls by carbon segregation from nickel nanoparticles. *ACS Nano* 8:6803–6811. doi:[10.1021/nn301546z](https://doi.org/10.1021/nn301546z)
- Yoon JC, Lee JS, Kim SI, Kim KH, Jang JH (2013) Three-dimensional graphene nano-networks with high quality and mass production capability via precursor-assisted chemical vapor deposition. *Sci Rep* 3:1788. doi:[10.1038/srep01788](https://doi.org/10.1038/srep01788)
- Yu QK, Lian J, Siriponglert S, Li H, Chen YP, Pei SS (2008) Graphene segregated on Ni surfaces and transferred to insulators. *Appl Phys Lett* 11:113103. doi:[10.1063/1.2982585](https://doi.org/10.1063/1.2982585)
- Zhao MQ, Zhang Q, Huang JQ, Tian GL, Nie JQ, Peng HJ, Wei F (2014) Unstacked double-layer templated graphene for high-rate lithium-sulphur batteries. *Nat Commun* 5:3410. doi:[10.1038/ncomms4410](https://doi.org/10.1038/ncomms4410)
- Zhong MJ, Jiang SY, Tang YF, Gottlieb E, Kim EK, Star A, Matyjaszewski K, Kowalewski T (2014) Block copolymer-templated nitrogen-enriched nanocarbons with morphology-dependent electrocatalytic activity for oxygen reduction. *Chem Sci* 5:3315–3319. doi:[10.1039/C4SC01477D](https://doi.org/10.1039/C4SC01477D)